

Scaling relations for globular cluster systems. Preliminary results for properties up to the effective radius

J.P. Caso^{1,2}, A.I. Ennis^{3,4}, B.J. De Bórtoli^{1,2} & L.P. Bassino^{1,2}

¹ *Facultad de Ciencias Astronómicas y Geofísicas, UNLP, Argentina*

² *Consejo Nacional de Investigaciones Científicas y Técnicas, Argentina*

³ *Waterloo Centre for Astrophysics, University of Waterloo, Canada*

⁴ *Perimeter Institute for Theoretical Physics, Waterloo, Canada*

Contact / jpcaso@fcaglp.unlp.edu.ar

Resumen / La interpretación de las relaciones de escala entre los sistemas de cúmulos globulares (SCG) y sus galaxias anfitrionas es relevante para develar los procesos físicos que rigieron su evolución. Hemos derivado los perfiles radiales de los SCG para un conjunto de galaxias masivas de tipo temprano que, junto a aquellas analizadas en nuestros trabajos previos, constituye una muestra homogénea, que abarca desde galaxias enanas hasta galaxias centrales de cúmulos. En esta contribución presentamos resultados preliminares del análisis de las propiedades de la región interna de los SCG.

Abstract / The analysis of the scaling relations between globular cluster systems (GCSs) and their host galaxies is relevant for our knowledge of the physical processes that ruled their evolution. We have calculated the radial profile of the GCS for a sample of massive early-type galaxies that, together with those presented in our previous articles, constitute a homogeneous sample, spanning from dwarfs to central galaxies in clusters. In this contribution we present preliminary results of the analysis of properties in the inner region of GCSs.

Keywords / galaxies: star clusters: general — galaxies: elliptical and lenticular, cD — galaxies: clusters: general

1. Introduction

Globular clusters (GCs) are considered as the massive end in the mass function of stellar clusters. Most of them were formed 8 – 10 Gyrs ago (e.g. Usher et al., 2019; Fahrion et al., 2020), at the maximum peak of star formation (Madau & Dickinson, 2014). The extreme environmental conditions that lead to their origin might also favour their disruption during the first Gyr after cluster formation (Li & Gnedin, 2019). In this scenario, merger episodes played a key role to redistribute them to the halo of the host galaxy (Kruijssen, 2015). Then, the build-up of globular cluster systems (GCSs) is tightly related to the merging history of their host galaxies (e.g. Kruijssen et al., 2019; Choksi & Gnedin, 2019). This is particularly relevant for bright early-type galaxies (ETGs), whose GCSs are the result of a two-phase process, with the *in-situ* population being enriched by GCs from accreted satellites (e.g. Forbes et al., 2011; Caso et al., 2017; El-Badry et al., 2019).

Hence, the fact that GCSs observed in the nearby Universe are conformed by the remaining objects of massive starburst episodes should not be overlooked, and many properties of GCs as well as their scaling relations at $z = 0$ should be interpreted in this context (e.g. Mieske et al., 2014; Rossi et al., 2016; Choksi & Gnedin, 2019). In this sense, literature results show that the average half-light radius of GCs seems to correlate with galactocentric distances (r_{gal} , Jordán et al. 2005), and the turn-over magnitude of the GC luminosity function (GCLF) in massive cluster galaxies becomes

fainter for larger values of r_{gal} (Harris et al., 2014). Both of these relations can be interpreted as evidence of the greater influence of tidal interactions in the disruption of GCS towards intergalactic medium. Although the inner regions of massive galaxies constitute a test bench for GC disruption, there are only few results about the inner part of the GCSs radial distribution in the literature (e.g. Brockamp et al., 2014; Capuzzo-Dolcetta & Mastrobuono-Battisti, 2009).

In this article we present preliminary results of the analysis of the inner GCS radial profile for a sample of massive and nearby ETGs. They complement our previous studies about scaling relations in ETGs, Caso et al. (2019) and De Bórtoli et al. (2022), hereafter Paper I and II, respectively, with the aim of contributing to the understanding of the processes that rule the evolution of GCSs and their host galaxies.

2. Observations and reduction

The data set consists of observations for a sample of nine galaxies from Virgo (programme 9401 Côté et al., 2004) and Fornax (programme 10217, Jordán et al., 2007) clusters, carried out with the ACS Wide Field Camera, mounted at the Hubble Space Telescope, and available at the Mikulski Archive for Space Telescopes* (MAST). The filters are $F475$ and $F850$, widely used to select and analyse GC candidates.

*<https://archive.stsci.edu/>

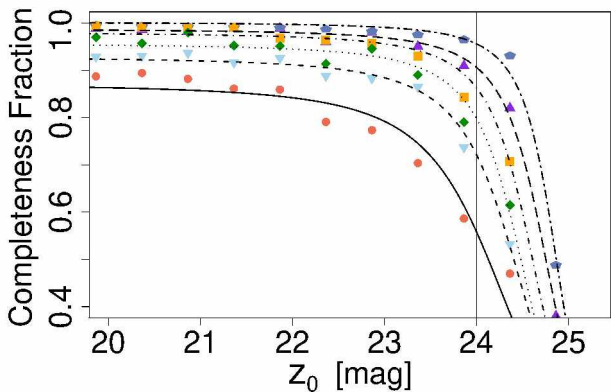


Figure 1: Completeness as a function of z_0 for M87. The completeness curves were calculated in different ranges of galactocentric distance (r_{gal}). The vertical line at $z_0 = 24$ mag indicates the assumed magnitude limit.

2.1. Photometry

The tasks ELLIPSE and BMODEL within IRAF are used to model the smoothed brightness distribution of the galaxy, which is subtracted to the original image. The detection of sources is performed with SOURCEEXTRACTOR (Bertin & Arnouts, 1996), using the same selection parameters as in Paper I. The aperture photometry for the point-sources is performed by means of DAOPHOT within IRAF, with an aperture radius of 5 px. Aperture corrections are calculated for each filter, from bright and relatively isolated point-sources.

2.2. Calibration, extinction correction and GC candidates selection

The instrumental magnitudes ($F475$, $F850$) are calibrated following the expressions from Sirianni et al. (2005), corresponding to magnitudes in g and z bands, respectively. Corrections for Galactic extinction are obtained from Schlafly & Finkbeiner (2011). Finally, GC candidates are chosen by their colour, fulfilling $0.6 < (g - z)_0 < 1.7$, a typical range for extragalactic GCs (see Paper I and references therein).

2.3. Completeness analysis

The photometric completeness for each galaxy is obtained by adding artificial stars to the images in both bands. Typically, 50 artificial stars are added per image, spanning the colour range of GCs and $20 < z_0 < 25.5$, and the process is repeated to achieve a final sample of 120 000 artificial stars. The photometry is performed in the same manner as in the science fields. The recovered artificial stars are used to build completeness curves in several ranges of r_{gal} (see Fig 1). The magnitude limit is chosen at $z_0 = 24$ mag, based on the drop in completeness for fainter objects.

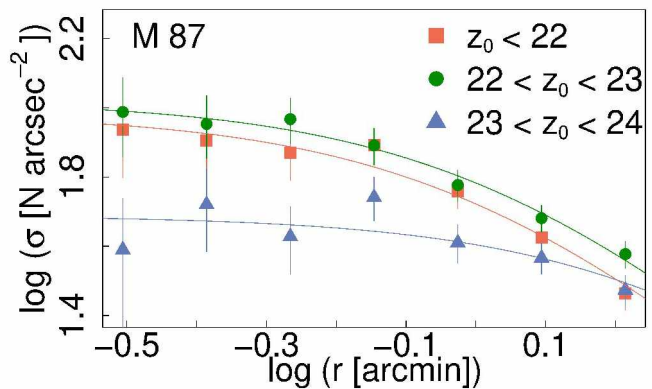


Figure 2: Radial profile for GC candidates, centred on M87, split in three different magnitude ranges. The solid curves represent modified Hubble profiles, fitted to the data.

3. Results

3.1. Radial distribution

The radial profiles of the GC candidates around the galaxies in our sample are obtained from concentric circular rings. At each bin, the corresponding completeness curve is used to correct the density. Several functions are used in the literature to fit radial profiles, including power-law and Sérsic profiles (Sersic, 1968). In this case, we choose the modified Hubble profile (Binney & Tremaine, 1987) which behaves as a power-law for large r_{gal} , and presents a central core that allows us to quantify the depletion of GCs in the inner regions of the galaxies. Considering the limited field-of-view of the HST/ACS images, and the typical extension of the GCSs in massive galaxies, the exponent of the profile is obtained from large scale studies from the literature, and only the scale radius of the core ($r_{0,\text{GCS}}$) and the central density are fitted.

Besides, in the most populated GCSs the GCs are separated into brightness intervals, and their radial profiles are fitted in the same manner as for the entire sample. For instance, Fig. 2 presents the radial profiles for three magnitude ranges of the GCS associated to M87. The radial profile corresponding to the faintest range presents a larger scale radius, $r_{0,\text{GCS}}$. This behaviour is in agreement with the GC erosion being driven by tidal disruption, which affects low-mass GCs more severely, rather than dynamical friction.

3.2. Comparison with properties of the host galaxy

The left panel in Fig. 3 shows the ratio between $r_{0,\text{GCS}}$ and the effective radius of the host galaxy, $r_{\text{eff,gal}}$, as a function of the stellar mass of the galaxy, M_* . The latter is obtained from the K magnitude of the galaxies available in NASA/IPAC Extragalactic Database**, and the mass-to-light ratios (M/L) derived by Bell et al. (2003). The red filled circles correspond to the galaxies analysed in this work, and the blue open ones represent the intermediate-mass galaxies from Papers I and II. In the vast majority of cases, the ratios range from 0.5 to

**<https://ned.ipac.caltech.edu/classic/>

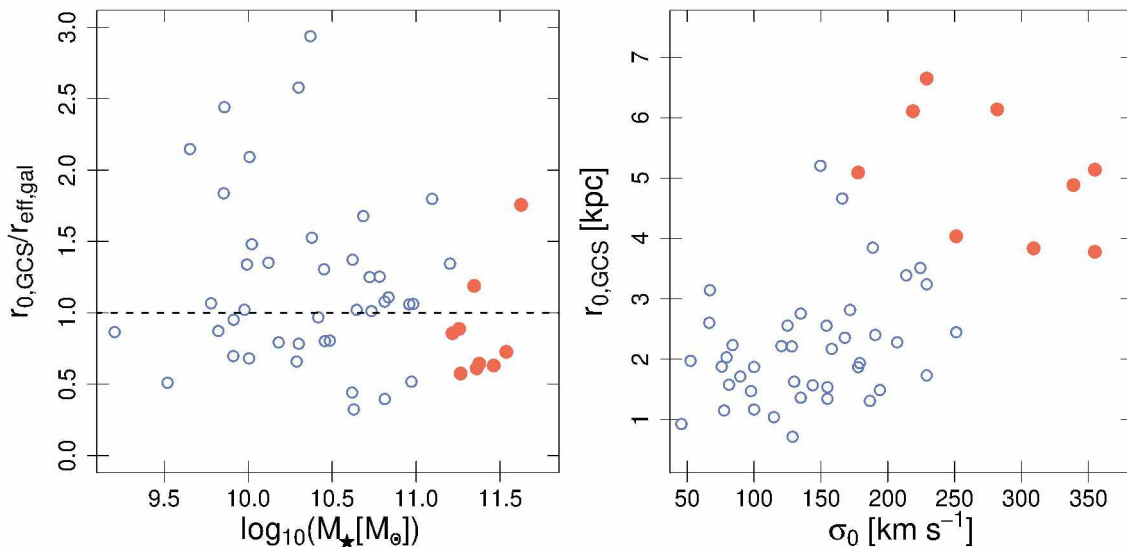


Figure 3: *Left panel:* ratio between the scale radius of the GCS, $r_{0,\text{GCS}}$, and the effective radius of the host galaxy, $r_{\text{eff,gal}}$, as a function of the stellar mass of the galaxy, M_* . The red filled circles correspond to the galaxies analysed in this work, and the blue open ones represent the intermediate-mass galaxies from Papers I and II. The dashed line is only for comparison purposes. *Right panel:* $r_{0,\text{GCS}}$ as a function of the central velocity dispersion of the host galaxy, (σ_0), symbols follow the same coding than the previous panel.

1.5, suggesting that both quantities are proportional. Although for massive galaxies ratios below one might prevail, the trend seems to span over two orders of magnitude in stellar mass. This implies a coeval evolution of the radial distribution for the GCS and the galaxy population, which is in agreement with the prediction from Brockamp et al. (2014).

The right panel presents the parameter $r_{0,\text{GCS}}$ as a function of the central velocity dispersion of the host galaxy (σ_0). The symbols follow the same coding as the previous panel. For GCSs in galaxies with σ_0 between 50 and 150 km s^{-1} (corresponding to intermediate-mass galaxies), the scale radius of the core does not vary significantly with σ_0 , but it increases for larger values of σ_0 (i.e., massive galaxies). Considering that σ_0 can be assumed as invariant to environmental processes (Spindler & Wake, 2017), the behaviour for massive galaxies could be related to the profusion of accretions and mergers in these galaxies, and their influence in redistributing GCs to the halo.

4. Summary

In this work we presented preliminary results of the analysis of radial profiles of GCSs associated with a sample of nearby massive galaxies. From the radial distribution of GCSs, the scale radius of the modified Hubble profile seems to increase for fainter GCs, suggesting a larger disruption towards lower masses. If no restriction on the brightness of the GCs is assumed, this parameter correlates with the effective radius of the host galaxy but presents a more complex behaviour as a function of its central velocity dispersion. Both of these relations denote a coeval evolution between the GCS and the un-

derlying stellar population of the galaxy. Our results also suggest the relevance of tidal disruption in eroding the inner GCS, and past mergers to redistribute GCs to the halo. Further analysis on a larger sample is needed to confirm our results.

References

- Bell E.F., et al., 2003, *ApJS*, 149, 289
- Bertin E., Arnouts S., 1996, *A&AS*, 117, 393
- Binney J., Tremaine S., 1987, *Galactic dynamics*
- Brockamp M., et al., 2014, *MNRAS*, 441, 150
- Capuzzo-Dolcetta R., Mastrobuono-Battisti A., 2009, *A&A*, 507, 183
- Caso J.P., Bassino L.P., Gómez M., 2017, *MNRAS*, 470, 3227
- Caso J.P., et al., 2019, *MNRAS*, 488, 4504
- Choksi N., Gnedin O.Y., 2019, *MNRAS*, 488, 5409
- Côté P., et al., 2004, *ApJS*, 153, 223
- De Bortoli B.J., et al., 2022, *MNRAS*, 510, 5725
- El-Badry K., et al., 2019, *MNRAS*, 482, 4528
- Fahrion K., et al., 2020, *A&A*, 637, A27
- Forbes D.A., et al., 2011, *MNRAS*, 413, 2943
- Harris W.E., et al., 2014, *ApJ*, 797, 128
- Jordán A., et al., 2005, *ApJ*, 634, 1002
- Jordán A., et al., 2007, *ApJS*, 169, 213
- Kruijssen J.M.D., 2015, *MNRAS*, 454, 1658
- Kruijssen J.M.D., et al., 2019, *MNRAS*, 486, 3180
- Li H., Gnedin O.Y., 2019, *MNRAS*, 486, 4030
- Madau P., Dickinson M., 2014, *ARA&A*, 52, 415
- Mieske S., Küpper A.H., Brockamp M., 2014, *A&A*, 565, L6
- Rossi L.J., Bekki K., Hurley J.R., 2016, *MNRAS*, 462, 2861
- Schlafly E.F., Finkbeiner D.P., 2011, *ApJ*, 737, 103
- Sersic J.L., 1968, *Atlas de Galaxias Australes*
- Sirianni M., et al., 2005, *PASP*, 117, 1049
- Spindler A., Wake D., 2017, *MNRAS*, 468, 333
- Usher C., et al., 2019, *MNRAS*, 490, 491